

Three-dimensional Distorted Born Iterative Method Enhanced by Breast Boundary Extraction for Microwave Mammography

Kazuki Noritake¹ and Shouhei Kidera¹

Abstract—Microwave mammography has several advantages *e.g.* portability, non-contact and cell-friendly measurement, and low cost for the equipment. Therefore, this technology has been regarded as a more frequent screening technique, than the X-ray based modality. This paper focuses on the dependence of the imaging accuracy, which is obtained using inverse scattering algorithms, on the estimation of the breast boundary. The Envelope method has been proposed as a method of using microwaves to estimate the location of the breast boundary. The accuracy of the boundary estimation via the Envelope method depends on that of the time-delay estimation, which is mostly processed by a filter based on waveform matching between the observed and reference signals. However, the coupling effect between the antenna and breast surface deforms the observed waveforms relative to the reference waveform. To mitigate this problem, this paper introduces the finite-difference time-domain (FDTD)-based waveform correction assuming the three-dimensional (3-D) distorted Born iterative method (DBIM) analysis. The 3-D numerical simulations based on realistic breast phantoms demonstrate that the proposed method enhances the accuracy for the 3-D reconstruction of the dielectric profile in highly heterogeneous cases.

Index Terms—Microwave mammography, Distorted born iterative method (DBIM), Envelope-based boundary extraction, FDTD-based waveform correction.

I. INTRODUCTION

According to the World Cancer Research Fund (WCRF)[1], breast cancer is the most widely diagnosed type of cancer in women. X-ray mammography is the most popular screening technique for the detection of breast-cancer tumors. However, X-ray mammography presents a risk of harming the cells and demands that the patient's breasts be subjected to high compression. The unpleasantness of the technique leads to low voluntary examination rates, particularly among young women. Although it is still in the research stage, microwave mammography has attracted considerable attention, being a cell-friendly and compact screening technique that is much less physically pain for the patient.

According to an examination of excised breast samples, there is a significant contrast between the dielectric properties of normal tissues (adipose dominant) and malignant tumors[2]. Many imaging algorithms have been developed for tumor detection or characterization; these can be divided into the following two categories as confocal (*e.g.*

beamforming[3]) and inverse scattering algorithms (*e.g.* Born approximation or distorted Born iterative method (DBIM)[4], contrast source inversion (CSI)[5]). This paper focuses on the DBIM, the effectiveness of which has been demonstrated in number of studies, even if the object has a highly heterogeneous and dispersive. However, the performance of the DBIM is extremely sensitive to the initial estimate of the dielectric property map and the region of interest (ROI), *i.e.*, the breast boundary[6][7]. Several ROI estimation algorithms are used in medical imaging, such as that based on the resonant frequency shift between the antenna and skin [8]. As a representative ROI estimation algorithm for breast media, the Envelope method has been introduced in the number of studies[9]. Additionally, a similar algorithm specifying the breast boundary, referred to as breast surface identification (BSID), has also been introduced in the literature [10], [11]. However, it should be noted that the successful reconstruction of ROI by the Envelope method relies on the accuracy of the estimations of the range between the antenna and breast surface. In the case of microwave mammography, the range between the antenna and skin surface is within the central wavelength, so the observed waveform is distorted compared to the reference waveform because of the near-field effect or the coupling effect. This waveform mismatch leads to a non-negligible error for range estimation based on waveform matching based filter, *e.g.* a matched filter.

To address the aforementioned issue, a previous study[12] proposed a direct compensation scheme for breast boundary estimation using the recovered FDTD recovered signal. Compensation for the range error can be applied directly by assessing the time-shift between the observed and recovered FDTD signals, for which the near-field effect should be considered. This paper extends this method to the three-dimensional (3-D) model, where the multi-static Envelope method is introduced to compensate the reconstruction error of ROI due to sparse array model. The results of FDTD-based numerical simulation using MRI-derived realistic numerical phantoms demonstrate that the proposed algorithm enhances the reconstruction accuracy of the DBIM outputs for highly heterogeneous breast media.

II. OBSERVATION MODEL

Figure 1 shows the observation model, assumed in the proposed method. Multiple transmitters and receivers array are located along the circumference curve, which surrounds an object area. The breast medium is comprised of skin, adipose, fibro-glandular, and tumor tissues, each of which

¹Graduate School of Informatics and Engineering, University of Electro-Communications, Japan
noritake.kazuki@ems.cei.uec.ac.jp
kidera@uec.ac.jp

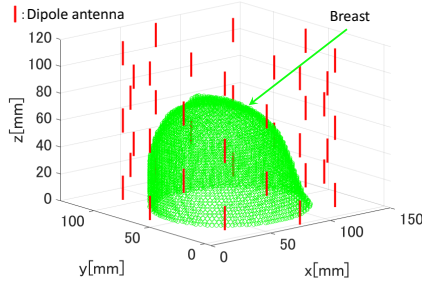


Fig. 1: Observation model.

have a lossy, dispersive, and isotropic dielectric properties. $E^{\text{scat}}(\mathbf{r}_t, \mathbf{r}_r; t)$ denotes the observed scattered electric field at the time t , where \mathbf{r}_t and \mathbf{r}_r denote the locations of transmitter and receiver, respectively.

III. DISTORTED BORN ITERATIVE METHOD (DBIM)

An electric field for each sensor location from dielectric media or object is formulated by the Helmholtz type integral equation[13]. Here, focusing on the scattered field $E^{\text{scat}}(\mathbf{r}_t, \mathbf{r}_r, \omega)$, which is observed at the receiver located at \mathbf{r}_r from the transmitter located at \mathbf{r}_t , the following integral equation holds:

$$\begin{aligned} E^{\text{scat}}(\mathbf{r}_t, \mathbf{r}_r, \omega) &\equiv E^{\text{total}}(\mathbf{r}_t, \mathbf{r}_r, \omega) - E^{\text{in}}(\mathbf{r}_t, \mathbf{r}_r, \omega) \\ &= \omega^2 \mu \int_{\Omega} G_0(\mathbf{r}', \mathbf{r}_r, \omega) E^{\text{total}}(\mathbf{r}_t, \mathbf{r}', \omega) o(\mathbf{r}') d\mathbf{r}', \end{aligned} \quad (1)$$

where Ω denote the region of interest (ROI) including an object, $E^{\text{scat}}(\mathbf{r}_t, \mathbf{r}_r, \omega)$ and $E^{\text{total}}(\mathbf{r}_t, \mathbf{r}_r, \omega)$ are the scattered and total electric fields, respectively, and $E^{\text{in}}(\mathbf{r}_t, \mathbf{r}_r, \omega)$ is the incident field in the presence of the background media with complex permittivity as $\epsilon_0(\mathbf{r})$, $G_0(\mathbf{r}', \mathbf{r}_r, \omega)$ is the Green's function assuming the background media, and $o(\mathbf{r}) = \epsilon(\mathbf{r}) - \epsilon_0(\mathbf{r})$ denotes the object function, where $\epsilon(\mathbf{r})$ is the complex relative permittivity of target. Here, ΔE^{total} is defined as:

$$\begin{aligned} \Delta E^{\text{total}}(\mathbf{r}_t, \mathbf{r}_r, \omega) &\equiv E^{\text{total}}(\mathbf{r}_t, \mathbf{r}_r, \omega) - E_b^{\text{total}}(\mathbf{r}_t, \mathbf{r}_r, \omega) \\ &= \omega^2 \mu \int_{\Omega} G_b(\mathbf{r}', \mathbf{r}_r, \omega) E^{\text{total}}(\mathbf{r}_t, \mathbf{r}', \omega) \Delta o(\mathbf{r}') d\mathbf{r}', \end{aligned} \quad (2)$$

where $G_b(\mathbf{r}', \mathbf{r}_r, \omega)$ is the Green's function of the background medium, $\Delta o(\mathbf{r}) = o(\mathbf{r}) - o_b(\mathbf{r})$ and $o_b(\mathbf{r})$ is the object function of background. Here, assuming that $\Delta o(\mathbf{r})$ is sufficiently small, $E^{\text{total}}(\mathbf{r}_t, \mathbf{r}', \omega) \simeq E_b^{\text{total}}(\mathbf{r}_t, \mathbf{r}', \omega)$ holds, and Eq. (2) is approximated as:

$$\begin{aligned} \Delta E^{\text{total}}(\mathbf{r}_t, \mathbf{r}_r, \omega) &\simeq \\ &\omega^2 \mu \int_{\Omega} G_b(\mathbf{r}', \mathbf{r}_r, \omega) E_b^{\text{total}}(\mathbf{r}_t, \mathbf{r}', \omega) \Delta o(\mathbf{r}') d\mathbf{r}'. \end{aligned} \quad (3)$$

The DBIM sequentially updates $o_b(\mathbf{r})$, $G_b(\mathbf{r}', \mathbf{r}_r, \omega)$ and $E_b^{\text{total}}(\mathbf{r}_t, \mathbf{r}_r, \omega)$ in order to minimize $|\Delta E^{\text{total}}(\mathbf{r}_t, \mathbf{r}_r, \omega)|^2$. To deal with dispersive media, its frequency dependency, denoted as Debye parameter, can be determined by exploiting the multiple frequency results[4][14].

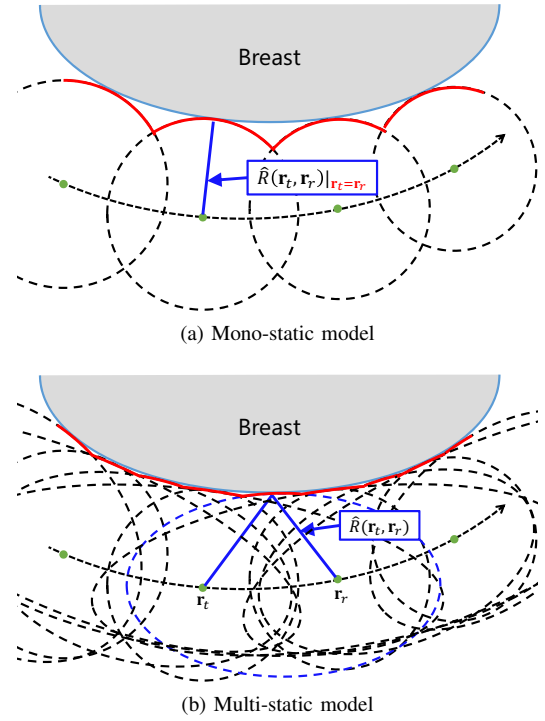


Fig. 2: Relationship between breast surface and outer envelope of ellipses. (a): Mono-static model. (b): Multi-static model. Red line shows the estimated boundary by each Envelope method.

Some studies revealed that while the DBIM accurately reconstruct the complex permittivity map having higher contrast, its accuracy has been highly dependent on that of the ROI estimation. Assuming the actual scenario, the breast boundary, namely the ROI boundary, should be preliminarily estimated by an appropriate imaging process.

IV. BOUNDARY EXTRACTION ENHANCED DBIM

A. Multi-static extended Envelope method

As a one promising solution for a prior estimate of breast boundary, we introduce the Envelope method, the effectiveness of which has been demonstrated in some observation models[9]. The principle of the Envelope method is very simple that an convex-shaped breast surface can be expressed as outer envelope of ellipsoids with its foci (origins of ellipsoids) as the transmitting and receiving antenna location and major radius as the distance between the antenna and skin surface.

In some literature as in [15], the multi-static extended Envelope method can enhance the accuracy boundary extraction with same computational complexity required in the mono-static based Envelope method. In particular, in the 3-D observation model, we need to consider the sparse array arrangement. Thus, to maintain the reconstruction accuracy of the breast surface, we introduce the multi-static extended Envelope method as follows. Figure 2 shows the principle of Envelope-based surface extraction, assuming the mono- and multi-static observation models. As shown in this figure,

the multi-static model could offer the interpolation effect compared with that obtained by the mono-static approach. Here, the range measured at the antenna location $(\mathbf{r}_t, \mathbf{r}_r)$ is defined as $\tilde{R}(\mathbf{r}_t, \mathbf{r}_r)$. $\tilde{R}(\mathbf{r}_t, \mathbf{r}_r)$ can be extracted from the local maximum of the output of the filter (*e.g.* matched filter) using a specific reference signal $E^{\text{ref}}(t)$. It is obvious that the shape estimation by the Envelope method relies on accurate range extraction as $\tilde{R}(\mathbf{r}_t, \mathbf{r}_r)$. The range measurement accuracy relies on the similarity of waveforms between the observed and assumed reference signals. Since the antennae and the breast surface are not separated more than a central wavelength of the transmitted pulse, the observed waveform includes a near-field component, incurring waveform deformation from the reference waveform.

B. FDTD-based waveform matching

To overcome the inaccuracy due to near-field observation model, this paper introduces the FDTD-based waveform reconstruction. The FDTD is one of most accurate forward solver by solving the differential form of Maxwell's equation. To compensate the error of range estimation due to using the initial reference signal assuming the far-field measurement, the reference signal is updated by the FDTD method, where the breast boundary is given by the initial estimate of the Envelope method. Naturally, the FDTD-recovered signal $\tilde{E}^{\text{obs}}(\mathbf{r}_t, \mathbf{r}_r; t)$, includes the near-field component, it is expected that the updated reference signal can enhance the accuracy in range estimation. This method directly updates the range as;

$$\hat{R}(\mathbf{r}_t, \mathbf{r}_r) = \tilde{R}(\mathbf{r}_t, \mathbf{r}_r) + c\Delta\tilde{\tau}(\mathbf{r}_t, \mathbf{r}_r)/2, \quad (4)$$

where c is the speed of light in the air, and $\Delta\tau(\mathbf{r}_t, \mathbf{r}_r)$ is calculated as;

$$\Delta\tilde{\tau}(\mathbf{r}_t, \mathbf{r}_r) = \arg \max_{\tau} [E^{\text{obs}}(\mathbf{r}_t, \mathbf{r}_r; t) \star \tilde{E}^{\text{obs}}(\mathbf{r}_t, \mathbf{r}_r; t)](\tau), \quad (5)$$

where \star denotes the operator of cross-correlation. ROI is also updated by the Envelope method using the group of $\hat{R}(\mathbf{r}_t, \mathbf{r}_r)$. It is expected that the boundary estimation performance of the Envelope method will also be upgraded by using the compensated ranges denoted as $\tilde{R}(\mathbf{r}_t, \mathbf{r}_r)$.

C. Incorporation DBIM and Envelope based Boundary Extraction

The actual procedure of the proposed method is presented as follows.

- Step 1) Observation data as $E^{\text{obs}}(\mathbf{r}_t, \mathbf{r}_r; t)$ are recorded at each combination of \mathbf{r}_t and \mathbf{r}_r , which is retrieved by the difference of total electric field between the case with and the case without object.
- Step 2) The boundary of ROI is estimated by the Envelope method using the group of $\tilde{R}(\mathbf{r}_t, \mathbf{r}_r)$.
- Step 3) Reference signal is updated using the FDTD method assuming a prior estimate of dielectric profile and ROI in Step 2).
- Step 4) Measured range for each antenna combination is updated in Eqs. (4) and (5).

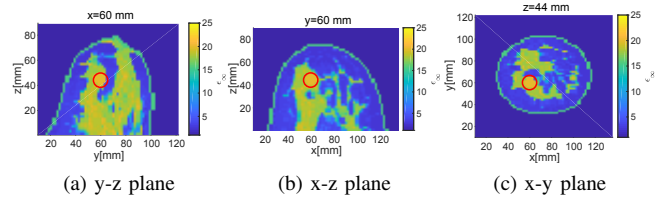


Fig. 3: 3-D numerical breast phantom (Class 3), where the color denotes the value of ϵ_{∞} . Red line : cancer location.

- Step 5) The boundary of ROI is estimated by the Envelope method using the group of $\hat{R}(\mathbf{r}_t, \mathbf{r}_r)$.
- Step 6) Steps from 2) to 5) are recursively done by the fixed iteration number.
- Step 7) Each Debye parameter is reconstructed by DBIM, where ROI is determined by the Step 6).

V. RESULT IN NUMERICAL TEST

The performance evaluation of the proposed method is assessed through the 3-D FDTD-based numerical simulation using realistic breast phantoms derived from MRI scans of healthy women [16]: Class 3 (Heterogeneously Dense) phantom. The frequency-dependent complex permittivities for the breast phantoms were modeled using the single-pole Debye model[2]. The scattered electric field is calculated by the FDTD method with single-pole Debye model (in-house code provided by the cross-disciplinary electromagnetics laboratory at the University of Wisconsin, Madison). Figure 3 illustrates the maps of the Debye parameters, ϵ_{∞} in Class 3 [16] which includes the 10mm size tumor with $(\epsilon_{\infty}, \Delta\epsilon, \sigma_s) = (20, 38, 0.8\text{S/m})$. Commercial software Remcom XFDTD Ver 7.6(Bio-Pro) was used for 3-D dispersive FDTD calculation. The transmitting signal formed a gaussian modulated pulse with a central frequency is 1.9 GHz, and a bandwidth is 2.8 GHz. The z -directed dipole antenna with 18 mm length is arranged cylindrically, surrounding the breast. The five array rings are set along z axis, where each array ring has 8 elements. All combination data as to transmitting and receiving antennae are processed in the DBIM. Each cell size in FDTD is 2mm. The conjugate gradient for least-squares (CGLS) method is used in the update of the dielectric profile in the DBIM, where the maximum iteration number is set to 100. Figure 4 shows the initial estimate map in the DBIM. Here, the initial The initial estimate of the dielectric property map is consist of skin, adipose and fibro-glandular tissues. Considering the typical spatial distribution of breast medium, it assumes that the skin layer with 2mm thickness is arranged along outer breast surface, and the adipose area is defined as the 20 mm inner area from the skin layer, and the remaining parts of breast is composed by the fibroglandular.

Figure 5 compares the waveforms for the observed, the initial reference, and the FDTD-recovered signals at the specific observation point. Figure 5 demonstrates that a similarity between $E^{\text{obs}}(t)$ and $\tilde{E}^{\text{obs}}(t)$ is considerably improved

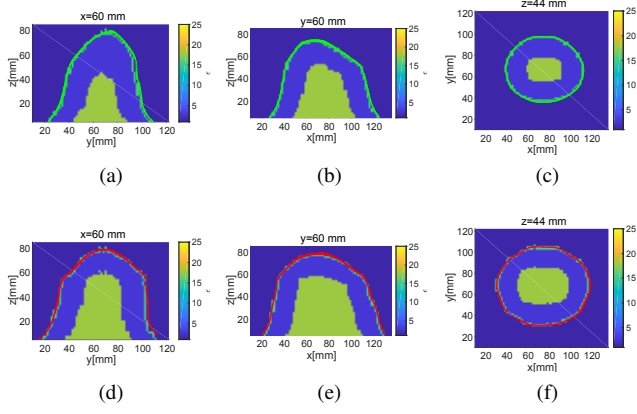


Fig. 4: Initial estimate map in the DBIM. (a)-(c):ROI is given by the Envelope without range compensation, (d)-(f):ROI is given by the Envelope with range compensation.

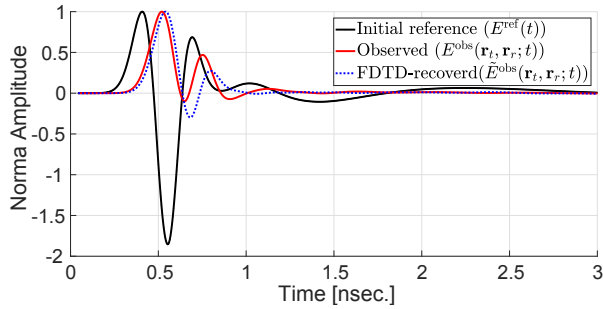


Fig. 5: Waveform comparison among observed signal $E^{\text{obs}}(\mathbf{r}_t, \mathbf{r}_r; t)$, initial reference signal and FDTD-recovered signal $\hat{E}^{\text{obs}}(\mathbf{r}_t, \mathbf{r}_r; t)$.

compared with that between $E^{\text{obs}}(t)$ and $E^{\text{ref}}(t)$. Figure 6 (a)-(c) shows a comparison of estimated outer boundary in the case using with or without the FDTD-based waveform compensation. Figure 6 shows that the proposed waveform compensation enhances the accuracy of 3-D breast boundary reconstruction. As a quantitative error analysis for the ROI estimation, the following criteria is introduced as;

$$\text{Err}_{\Omega} = \left| \int_{\Omega_{\text{true}}} dr - \int_{\hat{\Omega}} dr \right| / \int_{\Omega_{\text{true}}} dr, \quad (6)$$

where Ω_{true} and $\hat{\Omega}$ are the true ROI area and estimated ROI area. Then, $\text{Err}_{\Omega} = 7.07\%$ for the case without the FDTD-based waveform compensation. $\text{Err}_{\Omega} = 2.64\%$ for the case with the FDTD-based waveform compensation. This evaluation verifies that the proposed method considerably enhances the accuracy of the ROI estimation.

Figure 6 (d)-(i) shows the DBIM reconstruction results obtained using the ROI using the range with or without the FDTD-based waveform compensation. Here, for the quantitative analysis, the correlation coefficient (ρ) is introduced as;

$$\rho = \frac{(\mathbf{p}_{\text{true}}^T \mathbf{p}_{\text{est}})}{\|\mathbf{p}_{\text{true}}\|_2 \|\mathbf{p}_{\text{est}}\|_2}, \quad (7)$$

TABLE I: ρ and NRMSEs for each ROI.

ROI	ρ	NRMSE		
		ϵ_{∞}	$\Delta\epsilon$	σ_s
Estimated w/o comp.	0.5230	1.26	1.72	1.89
Estimated w/ comp.	0.6039	1.29	1.77	1.90
Given	0.7527	0.88	1.22	1.25

where $\mathbf{p} = [\epsilon_{\infty}^T \Delta\epsilon^T \sigma_s^T]^T$, \mathbf{p}_{true} , \mathbf{p}_{est} is true and estimated vector of Debye parameter. And also the normalized root mean square (NRMSE) is also introduced as;

$$\text{NRMSE}_{\hat{X}} = \frac{1}{\bar{X}_{\text{true}}} \sqrt{\frac{1}{K} \sum_{k=1}^K |\hat{X}(\mathbf{r}_k) - X_{\text{true}}(\mathbf{r}_k)|^2}, \quad (8)$$

where $\hat{X}(\mathbf{r}_k)$ and $X_{\text{true}}(\mathbf{r}_k)$ are the original and estimated values of the Debye parameter at each location \mathbf{r}_k , \bar{X}_{true} denotes the mean of $X_{\text{true}}(\mathbf{r})$, K is the total number of unknowns in ROI. Table I summarizes ρ and NRMSEs of DBIM's reconstruction results for each ROI. ρ verify that the proposed method considerably enhanced the accuracy of the DBIM estimation. The reason why the NRMSE is not upgraded is that the number of unknowns are considerably increased and the ill-posedness of the problem is more severe in th 3-D case.

VI. CONCLUSION

This paper have introduced accuracy enhanced DBIM based inverse scattering method by a prior estimate of the ROI based on the FDTD waveform compensation. The ROI estimation accuracy by the Envelope method was upgraded by the range error compensation by the updated reference signal using FDTD. Based on the 3-D FDTD numerical analysis, assuming the realistic breast phantom including cancer cell, demonstrated that our proposed method enhanced the accuracy of the 3-D DBIM inverse scattering analysis. Since the key point for enhancing the accuracy is the reduction of unknowns, we will introduce the basis function based reconstruction or the simplified but appropriate mathematical model to decrease the number of unknowns in our future work.

ACKNOWLEDGMENT

This research and development work was supported by the MIC/SCOPE #162103102.

REFERENCES

- [1] WCRF, "Diet, nutrition, physical activity and breast cancer", URL: <https://www.wcrf.org/sites/default/files/Breast-cancer-report.pdf>
- [2] M. Lazebnik, D. Popovic, L. McCartney, C. B. Watkins, M. J. Lindstrom, J. Harter, S. Sewall, T. Ogilvie, A. Magliocco, T. M. Breslin, W. Temple, D. Mew, J. H. Booske, M. Okoniewski, and S. C. Hagness, "A large-scale study of the ultrawideband microwave dielectric properties of normal, benign and malignant breast tissues obtained from cancer surgeries", *IOP Publishing Phys. Med. Biol.* vol. 52, pp. 6093–2093 2007.

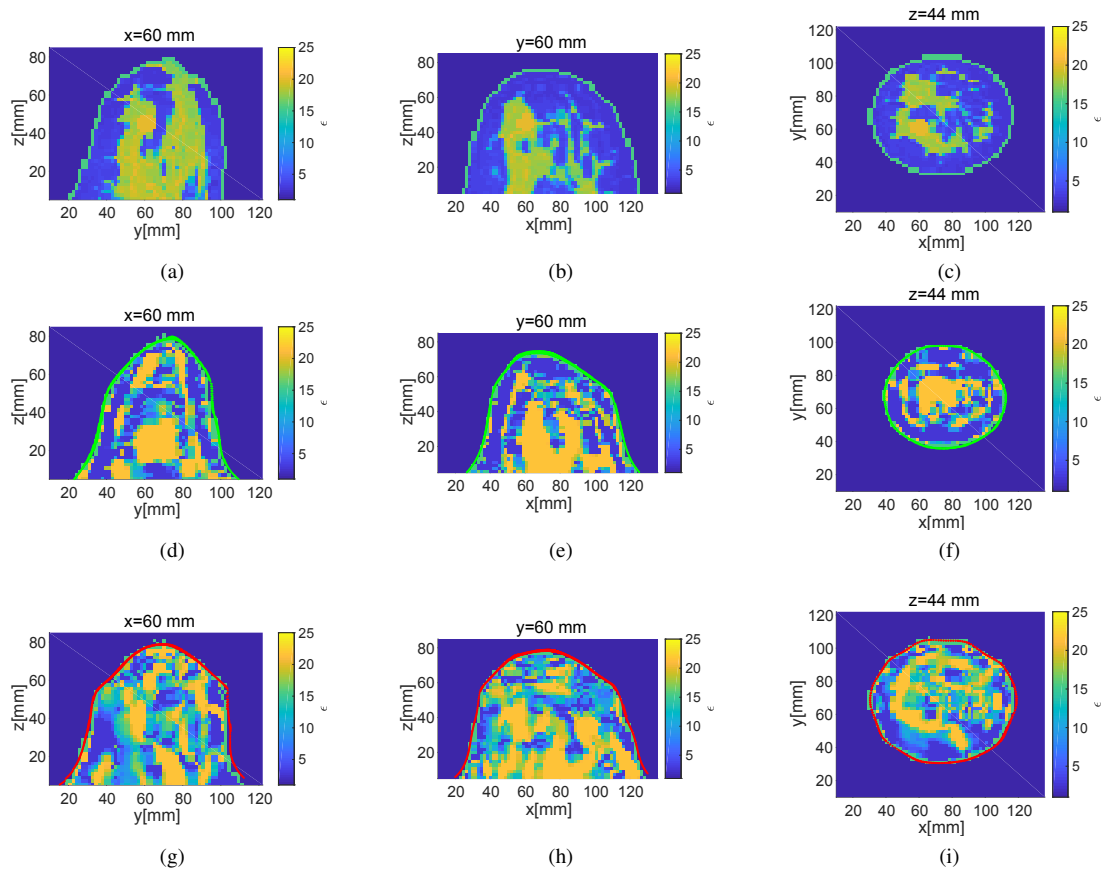


Fig. 6: Results of the reconstruction by DBIM. Green and red lines denote the ROI estimated without and with waveform compensation, respectively. (a-c): Original profile. (d-f): DBIM reconstruction without waveform compensation. (g-i): DBIM reconstruction with waveform compensation (proposed method).

- [3] E. J. Bond, Xu Li, and S. C. Hagness, "Microwave imaging via space-time beamforming for early detection of breast cancer", *IEEE Trans. Antennas Propag.*, vol. 1, no. 8, pp. 1690-1705, Aug. 2003.
- [4] J. D. Shea, P. Kosmas, S. C. Hagness and B. D. Van Veen., "Three-dimensional microwave imaging of realistic numerical breast phantoms via a multiple-frequency inverse scattering technique", *Am. Assoc. Phys. Med.*, vol. 37, no. 8, pp.4210-4226, Aug.2010.
- [5] P. M van den Berg and R. E Kleinmanz,"A contrast source inversion method", *IOP, Inverse Problems*, Vol.13, pp1607-1620, 1997.
- [6] F. Gao, B. D. Van Veen, and S. C. Hagness, "Sensitivity of the distorted Born iterative method to the initial guess in microwave breast imaging," *IEEE Transactions on Antennas and Propagation*, vol. 63, no. 8, pp. 3540-3547, Aug. 2015.
- [7] A. Fhager and M. Persson, "Reconstruction strategies for microwave imaging of breast; reconstructions constrained to the breast domain", *Microwave Bio Conference (IMBIOC)*, 2017.
- [8] A. Zamani, S. A. Rezaeieh, K. S. Bialkowski, A. M. Abbosh, "Boundary Estimation of Imaged Object in Microwave Medical Imaging Using Antenna Resonant Frequency Shift", *IEEE Trans. Antennas Propag.*, vol. 66, no. 2, pp. 927-936, Feb., 2018.
- [9] S. Kidera, T. Sakamoto, and T. Sato., "A Robust and Fast Imaging Algorithm with an Envelope of Circles for UWB Pulse Radars", *IEICE Trans Commun.*, vol. E90-B, no.7, pp.1801-1809, July.2007.
- [10] D. W. Winters, J. D. Shea, E. L. Madsen, G. R. Frank, B. D. Van Veen, and S. C. Hagness, "Estimating the breast surface using UWB microwave monostatic backscatter measurements", *IEEE Trans. Biomed. Eng.*, vol. 55, no.1, pp.247-255, Jan.2008.
- [11] M. Sarafianou, D.R. Gibbins, I.J. Craddock, M. Klemm, J.A. Leendertz, A. Preece, and R. Benjamin, "Breast Surface Reconstruction Algorithm for a Multi-Static Radar-Based Breast Imaging System", *Proc.4thEur. Conf. Antennas Propag.(EuCAP)*, 2010, pp1-5.
- [12] K. Noritake and S. Kidera, "Boundary Extraction Enhanced Inverse Scattering Method for Microwave Mammography", *12th European Conference on Antennas and Propagation (EuCAP 2018)*.
- [13] M. A. Fiddy and R. S. Ritter, 2014, "Introduction to Imaging from Scattered Fields", CRC Press.
- [14] T. J. Cui, W. C. Chew, A. A. Aydinler, and S. Chen,"Inverse Scattering of Two-Dimensional Dielectric Objects Buried in a Lossy Earth Using the Distorted Born Iterative Method", *IEEE Trans. Geosci. Remote Sens.*, vol. 39, no. 2, pp.339-346, Feb.2001.
- [15] S. Kidera, Y. Kani, T. Sakamoto and T. Sato, "Fast and Accurate 3-D Imaging Algorithm with Linear Array Antennas for UWB Pulse Radars", *IEICE Trans. Commun.*, vol.E91-B, no.8, pp. 2683-2691, Aug. 2008.
- [16] UWCEM, "Numerical breast phantom repository", URL:<https://uwcem.ece.wisc.edu/phantomRepository.html>